ELSEVIER

International Journal of Heat and Fluid Flow 19 (1998) 307–319

International Journal of HEAT AND FLUID FLOW

Computational prediction of flow around highly loaded compressor-cascade blades with non-linear eddy-viscosity models

W.L. Chen, F.S. Lien, M.A. Leschziner *

Department of Mechanical Engineering, UMIST, Manchester M60 1QD, UK

Received 7 March 1997; accepted 5 December 1997

Abstract

A computational study is presented which examines the predictive performance of two variants of a cubic low-Re eddy-viscosity model when applied to the flow around two highly loaded compressor-cascade blades. Particular challenges are posed by the transitional nature of the flow and the presence of laminar leading-edge separation in off-design conditions. Comparisons are presented for local as well as integral flow parameters, including turbulence intensity and losses. The study demonstrates that the cubic model is able to predict, in accord with experimental data and in contrast to a linear base-line model, the influential leading-edge separation preceding transition, due to the suppression of turbulence-energy generation in the impinging zone ahead of the leading edge. This attribute and a greater sensitivity to streamline curvature enable the model to give, in some flow conditions, a more realistic description of the development of the boundary layer after transition and a better prediction of the loss at off-design incidence. However, the model also exhibits predictive weaknesses, among them an inappropriate delay in reattachment and transition to fully developed turbulence, resulting in insufficient sensitivity to adverse pressure gradient once transition has occurred.

Keywords: Compressor cascade; Turbulence modelling; Non-linear eddy-viscosity closure; Transition; Off-design conditions

Notation

a_{ij}	deviatoric stress tensor
A_2	second invariant of stress tensor
C_p	surface-pressure coefficient
C	chord length
c_μ, f_μ	coefficients in eddy-viscosity relation
i	inlet-flow incidence angle
k	turbulence energy
l_ε	turbulence dissipation length scale
p	pressure
P_{T0}, P_{T2}	total pressure at inlet and outlet, respectively
P_{D1}	dynamic pressure at inlet
$\mathrm{Re_c}$, $\mathrm{Re_d}$	Reynolds numbers based on chord length and leading-edge diameter, respectively
R_t	local turbulence Reynolds number
$S_{ij}, \tilde{S}$	strain rate tensor and its invariant, $(k/\tilde{\varepsilon})(0.5S_{ij}S_{ij})^{0.5}$, respectively
Tu	inlet-flow turbulence intensity
$\overline{u_i'u_j'}$	Reynolds-stress tensor
u_i	velocity vector
x_i	Cartesian coordinates
y	normal distance from the wall
δ	boundary-layer thickness
δ_{ij}	Kronecker delta
ε	dissipation rate of k
$\tilde{\varepsilon}$	homogeneous dissipation rate of k, $\varepsilon - 2\nu(\partial\sqrt{k}/\partial x_i)^2$
β	inlet-flow angle
μ_t, ν_t	dynamic and kinematic turbulence viscosity
ρ	fluid density
$\Omega_{ij}, \tilde{\Omega}$	vorticity tensor and its invariant, $(k/\tilde{\varepsilon})(0.5\Omega_{ij}\Omega_{ij})^{0.5}$, respectively
ω	loss coefficient

1. Introduction

The principal aerodynamic characteristics of most turbomachine flows are governed mainly by a balance between pressure gradient and convection, while turbulence tends to affect mainly secondary flow features and the losses. This is at least so in low-load conditions in which the boundary layers are relatively thin and attached. In high-load and off-design conditions, however, turbulence can contribute substantially to the aerodynamic balance and is thus a process of major practical interest. In such circumstances, the boundary layers grow rapidly, separation can ensue on both suction and pressure sides (depending on the blade geometry and the incidence angle) and streamwise vorticity is intense – all processes interacting strongly with the turbulence structure. The sensitivity of major mean-flow features to turbulence is especially high when the flow enters the blade passage at an angle which departs

* Corresponding author. E-mail: m.leschziner@umist.ac.uk.

0142-727X/98/$19.00
PII: S0142-727X(98)10001-2

materially from the design value, thus causing leading-edge separation and high flow displacement, followed by transition in the separated shear layer. More generally, transition tends to be a highly influential process in the majority of off-design flows in that details of the location and evolution of transition can dictate the sensitive response of the boundary layers to pressure gradients.

The large majority of computational schemes for turbomachinery currently involve the use of the linear (Boussinesq) relationships between stresses and strains,

$$-\rho\overline{u_i'u_j'} = \mu_t\left(\frac{\partial u_i}{\partial x_j}+\frac{\partial u_j}{\partial x_i}\right)-\frac{2}{3}\rho k\delta_{ij} \tag{1}$$

coupled with algebraic expressions or, at most, differential equations for the turbulent velocity and length scales to which the turbulent viscosity is related. This framework is accepted as being adequate for thin shear flows and is able to reproduce transition in simple boundary layers (Savill, 1991), if combined with appropriately constructed and calibrated transport equations for the variation of the scales in low-Reynolds-number conditions. However, it fails to resolve turbulence anisotropy and to represent correctly the effects of normal straining and curvature on the turbulent stresses. The last two deficiencies are especially important in blade flows; first, because the state of turbulence at the leading-edge impingement region is crucially important to the transitional behaviour further downstream, and second, because the blade curvature causes significant damping or augmentation of turbulence transport in the boundary layers on the suction and pressure sides, respectively.

It is now generally accepted that the substantial variability in the strength of the interaction between different strain types and the turbulent stresses can only be resolved, in a fundamentally rigorous sense, through the use of second-moment closure, in which separate transport equations are solved for all Reynolds-stress components. In particular, the very different stress-generation terms contained in these equations give rise to that closure's ability to resolve anisotropy and hence the influence of curvature, rotation and normal straining on the stresses (Launder, 1989; Leschziner, 1994). However, this type of closure is complex, poses particular challenges in respect of its stable integration into general computational schemes and is costly to apply in practice (Lien and Leschziner, 1996). A simpler and more economical alternative – albeit one which rests on a weaker fundamental foundation – is to use non-linear stress–strain relations which can be made to return, upon the introduction of physical constraints and careful calibration, some of the predictive capabilities of second-moment closure.

The present paper considers the performance of two low-Re cubic eddy-viscosity models when applied to the flow around highly loaded compressor-cascade profiles. Among a number of issues, the resolution of laminar leading-edge separation and bypass transition – the latter either in the separated shear layer bordering the leading-edge bubble or in the attached boundary layer – is both challenging and highly influential to the overall predictive realism.

2. Turbulence modelling

Non-linear eddy-viscosity modelling has its origin in a general proposal made by Pope (1975). This was not, however, realized as part of a working model until the late 1980s when several specific non-linear forms were constructed and tested. Speziale (1987), Nisizima and Yoshizawa (1987), Rubinstein and Barton (1990) and Shih et al. (1993) have all introduced quadratic products of strain and vorticity tensors into the stress–strain relationship, but adopted different routes to their models' derivation and calibration. These quadratic forms return a degree of anisotropy among the normal stresses and hence are able to predict, among other features, the presence of stress-driven secondary motion in fully developed square-duct flow. However, it is readily demonstrated that no quadratic form is able to establish the correct sensitivity of the shear stresses to streamline curvature, one of the most important factors motivating the use of closures more complex than those based on the Boussinesq relationships. To introduce this sensitivity, Craft et al. (1993) proposed a non-linear form which includes cubic products of strain and vorticity tensors. They have also demonstrated the need to include cubic terms for swirling flows. More recently, Lien et al. (1995) have proposed a substantially simpler cubic variant, based on the quadratic model of Shih et al., while Apsley and Leschziner (1997) have derived a cubic model by introducing a rational sequence of approximations to second-moment closure and calibrating the low-Re near-wall behaviour by reference to DNS data. Finally, Lien and Durbin (1996) have investigated the use of a transport equation for the streamline-normal Reynolds stress as the subject of a third transport equation to which the coefficients of the non-linear stress–strain relations are sensitized.

In what follows, attention focuses on the two- and three-equation models of Craft et al. (1997) – the most elaborate variants currently documented in the open literature. These distinguish themselves from others in two important respects: first, while applicable to low-Re near-wall conditions, they do not involve wall-distances; second, they characterize the near-wall structure by the second anisotropy invariant $A_2 = \left(\overline{u_i'u_j'} - \frac{2}{3}k\delta_{ij}\right)^2$ and use this, in addition to the turbulence Reynolds number, to sensitise the eddy viscosity to wall-induced damping.

Although the rational foundation and derivation of different non-linear models varies, the constitutive stress–strain/vorticity relationship underlying all cubic models and satisfying the requisite symmetry and contraction properties for incompressible flow can be written as

$$\begin{aligned} a_{ij} \equiv \frac{\overline{u_i'u_j'}}{k}-\frac{2}{3}\delta_{ij} &= -\frac{\nu_t}{k}S_{ij} + c_1\frac{\nu_t}{\tilde{\varepsilon}}\left(S_{ik}S_{kj}-\frac{1}{3}S_{kl}S_{kl}\delta_{ij}\right) \\ &+ c_2\frac{\nu_t}{\tilde{\varepsilon}}\left(\Omega_{ik}S_{kj}+\Omega_{jk}S_{ki}\right) + c_3\frac{\nu_t}{\tilde{\varepsilon}}\left(\Omega_{ik}\Omega_{jk}-\frac{1}{3}\Omega_{lk}\Omega_{lk}\delta_{ij}\right) \\ &+ c_4\frac{\nu_t k}{\tilde{\varepsilon}^2}\left(S_{ki}\Omega_{lj}+S_{kj}\Omega_{li}\right)S_{kl} \\ &+ c_5\frac{\nu_t k}{\tilde{\varepsilon}^2}\left(\Omega_{il}\Omega_{lm}S_{mj}+S_{il}\Omega_{lm}\Omega_{mj}-\frac{2}{3}S_{lm}\Omega_{mn}\Omega_{nl}\delta_{ij}\right) \\ &+ c_6\frac{\nu_t k}{\tilde{\varepsilon}^2}S_{ij}S_{kl}S_{kl} + c_7\frac{\nu_t k}{\tilde{\varepsilon}^2}S_{ij}\Omega_{kl}\Omega_{kl}. \end{aligned} \tag{2}$$

In the simpler (two-equation) model of Craft et al., the coefficients, c_1 to c_7, have been optimized by reference to several flows, including homogeneous shear flows, swirling flows and curved-channel flows, and the resulting numerical values for the coefficients are given in Table 1.

It is instructive to note that, in two-dimensional plane flows, where only S_{11}, S_{22} and S_{12} exist, the term associated with c_4 vanishes, and Eq. (2) can be rewritten, with the coefficients in Table 1, as

Table 1
Numerical values for coefficients in the two-equation model of Craft et al

c_1	c_2	c_3	c_4	c_5	c_6	c_7
−0.1	0.1	0.26	$-10c_\mu^2$	0	$-5c_\mu^2$	$5c_\mu^2$

$$a_{ij} = -\left[\frac{v_t}{k} + 5c_\mu^2 \frac{v_t k}{\tilde{\varepsilon}^2}\left(S_{kl}^2 - \Omega_{kl}^2\right)\right] S_{ij} + \text{ quadratic terms.} \qquad (3)$$

The result (3) has been written in such a way as to highlight the fact that the cubic terms can be assimilated into the linear term, and this allows the effects of curvature to be brought out. Thus, the shear stress will increase when $S_{kl}^2 > \Omega_{kl}^2$ and will decrease when $S_{kl}^2 < \Omega_{kl}^2$. In the case of flow over a blade, the curved blade surfaces introduce significant streamline curvature, which makes $S_{kl}^2 \neq \Omega_{kl}^2$, and the influence of the cubic terms thus becomes significant. It is further instructive to note that in a simple plane shear layer, for which $S_{ij} = S_{12}$, Eq. (3) yields

$$a_{11} = 0.25\frac{v_t}{\tilde{\varepsilon}} S_{12}^2, \qquad a_{22} = -0.15\frac{v_t}{\tilde{\varepsilon}} S_{12}^2, \qquad (4)$$

which demonstrates the role of the quadratic terms in establishing the anisotropy of normal stresses.

The eddy viscosity is determined from

$$\mu_t = \rho f_\mu c_\mu \frac{k^2}{\tilde{\varepsilon}} \qquad (5)$$

in conjunction with transport equations for k and $\tilde{\varepsilon}$ (Craft et al., 1993). The value of c_μ has been calibrated by reference to DNS data for homogeneous-shear flow and has been made a function of strain and vorticity invariants as follows:

$$c_\mu = \frac{0.3}{1 + 0.35\{\max(\tilde{S}, \tilde{\Omega})\}^{1.5}} \times \left[1 - \exp\left\{\frac{-0.36}{\exp(-0.75\ \max(\tilde{S}, \tilde{\Omega}))}\right\}\right]. \qquad (6)$$

The term in square brackets in Eq. (6) is a damping function which forces c_μ to reduce to 0.09 when $\tilde{S}$ and $\tilde{\Omega}$ approach zero. Moreover, the appearance of $\tilde{S}$ in the denominator of Eq. (6) causes a significant reduction in the turbulence energy in regions with large values of $\tilde{S}$, such as around stagnation points, through the reduction of the c_μ value. This is, in fact, a key feature in relation to the model's ability to predict transition following leading-edge separation. The use of $\max(\tilde{S}, \tilde{\Omega})$ in Eq. (6) is aimed to preferentially enhance the sensitivity of the model to streamline curvature for convex surfaces for which $\tilde{\Omega} > \tilde{S}$, relative to the enhancement provoked by curvature on concave surfaces. The damping function f_μ has the form

$$f_\mu = 1 - \exp\left\{-\left(\frac{\tilde{R}_t}{90}\right)^{1/2} - \left(\frac{\tilde{R}_t}{400}\right)^2\right\}, \qquad (7)$$

which introduces a strong Reynolds-number dependence into the model and impinges on its ability to represent transition.

Craft et al. (1997) have recently developed an extension of the above model in which the coefficients are sensitized to the second invariant of the anisotropy A_2, the distribution of which is determined from the solution of a related transport equation derived from second-moment closure. They have justified this extension by the observation that the strain invariant is ineffective as a near-wall damping parameter, because its distribution is flat in the region of $y^+ > 40$, while some damping proves necessary up to $y^+ \approx 60$. In contrast, DNS results of Kim et al. (1987) show that A_2 varies substantially in the region of $y^+ < 60$, thus offering better potential for sensitizing the model to the strong anisotropy very close to the wall. A disadvantage of this three-equation model is its considerably greater complexity than the earlier form which only requires the solution of the k and $\tilde{\varepsilon}$ equations. This model is also much less robust, and it has been found impossible to apply it in extreme off-design conditions.

3. Numerical framework

Calculations reported herein have been performed with the multi-block version of the general non-orthogonal, fully collocated finite-volume approach 'STREAM' (Lien and Leschziner, 1994a, b; Lien et al., 1996). The type of grid topology that can be accommodated with the multi-block version is illustrated in Fig. 1 which relates to a controlled-diffusion compressor-cascade blade. The algorithm includes a flow-adaptive multi-level local grid-refinement capability (Chen et al., 1997a) which has been used in conjunction with the non-linear eddy-viscosity models outlined in Section 2. Convection of mean-flow as well as turbulence quantities is approximated with the scheme 'UMIST' (Lien and Leschziner, 1994c), a second-order TVD implementation of the QUICK scheme of Leonard (1979). The predicted onset and evolution of transition, especially in flat-plate flow, have been observed to be extremely sensitive to numerical details, and the retention of second-order accuracy for turbulence convection was therefore essential, even when very fine grids were used. Mass continuity is enforced indirectly by way of a pressure-correction algorithm. Within this scheme, the transport solutions and the pressure-correction equation are solved sequentially and iterated to convergence, defined by reference to Euclidean residual norms for mass and the momentum components.

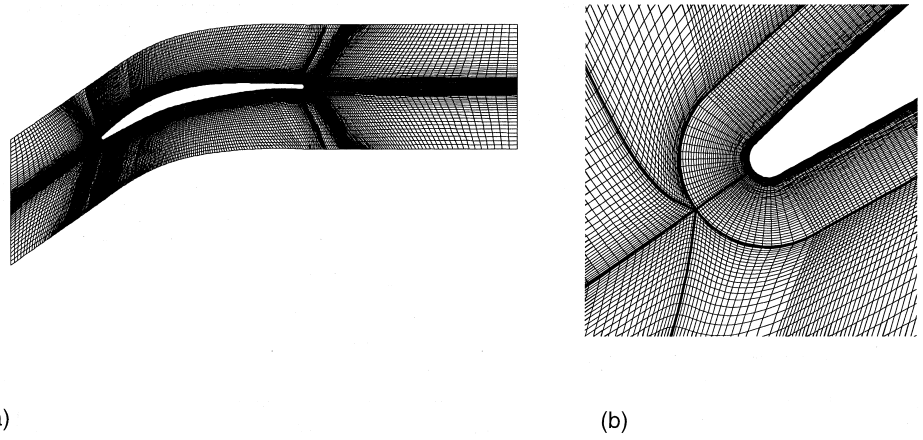

Fig. 1. Computational grid for CD compressor blade: (a) Computational mesh with 48 000 grid nodes. (b) Grid near the leading edge.

4. Application to compressor blades

4.1. Introductory remarks

The turbulence models outlined in Section 2 and the linear low-Re variant of Launder and Sharma (1974) – the last playing the role of a baseline model – are here applied to the flow around two compressor blades: a *Controlled Diffusion* (CD) blade investigated experimentally by Elazar and Shreeve (1990) and a *Double Circular Arc* (DCA) blade examined by Zierke and Deutsch (1989). The former flow is essentially attached, except for a laminar leading-edge separation. The latter case is considerably more complex, involving extensive separation in the passage and transition on the blade's surfaces, thus posing particular modelling challenges. The flow features leading-edge as well as trailing-edge separation. Mid-chord separation is also encountered in certain flow conditions, and the blade has much larger curvature than the CD configuration.

Attention is focused initially on the CD configuration. The aim is to elucidate some basic performance characteristics of the models and to identify any weaknesses in conditions which, while realistic, do not include the substantial complexities associated with extensive suction-side separation close to the trailing edge. With insight derived from this computation, attention is then directed towards the more complex flow over the DCA blade.

4.2. The CD blade – geometry and computed flow conditions

The CD blade investigated here was originally designed by Sanger (1983). Experiments have been performed by Elazar and Shreeve (1990) at three values of inlet-flow angle β, namely 40°, 43.4° and 46°. The first corresponds to the *near-design* state, while the second and the third give rise to increasing loading and are referred to as *off-design* conditions. Computations have been performed for the seven inlet angles and Reynolds numbers listed in Table 2 to investigate the performance of the turbulence models over a wide range of flow conditions. In this Table, the Axial Velocity Density Ratio (AVDR) is seen to be nearly unity for most of the cases, and this suggests that the global acceleration arising from the reduction in effective flow area due to the boundary layers developing on the spanwise walls is not significant. Hence, this effect has not been taken into account in the computations reported below. However, in a preliminary study, quasi-3D test computations were performed in which global spanwise effects were taken into account, and these yielded solutions very close to the corresponding 2D computations.

Table 2
CD blade – flow conditions investigated

Case no.	Flow angle (degree)	Re_c	AVDR
1	24.49	690 000	1.0209
2	28.00	648 000	1.0544
3	32.95	630 000	1.0738
4	37.07	683 000	1.0380
5	40.00	740 000	1.0250
6	43.4	774 000	1.0710
7	46.00	700 000	1.0600

Fig. 1 shows the multi-block computational mesh which surrounds the blade and extends, in the cross-stream direction, from the middle of one passage to the middle of the adjacent one. The mesh also extends to a distance of half of the chord upstream and one chord downstream of the blade. This mesh contains 48 000 grid nodes, and a particularly fine grid has been prescribed close to the leading edge to resolve the leading-edge separation bubble. There are 400 grid nodes distributed along the blade surfaces, and 200 grid nodes cover the flow passage in the pitchwise direction. The necessity of using such a fine mesh is demonstrated by the results of grid-independence tests shown in Fig. 2. These results were obtained with three grids containing 25 200, 48 000 and 58 000 grid nodes, respectively, with the two-equation cubic model at the inlet angle $\beta = 46°$. In this operational condition, there exists a large leading-edge separation bubble, and the suction side is subjected to a strong adverse pressure gradient which leads to a thick boundary layer as the trailing-edge is approached. Both processes require the use of a fine mesh to obtain an adequate numerical resolution. The suction-side velocity distributions given in Fig. 2 demonstrate that a grid-independent solution has been achieved with the mesh containing 48 000 grid nodes. With this mesh, the y^+ -values of the surface-nearest grid nodes are well below unity.

An important requirement, especially in the context of transitional flows, is that the predicted variation of turbulence intensity outside the boundary layers accords well with that measured. In fact, this comparison provides the only means of selecting the appropriate levels of turbulence energy and dissipation-length scale at the computational inlet plane, which ensure that the free-stream turbulence intensity at the boundary-layer edge is in satisfactory agreement with the experi-

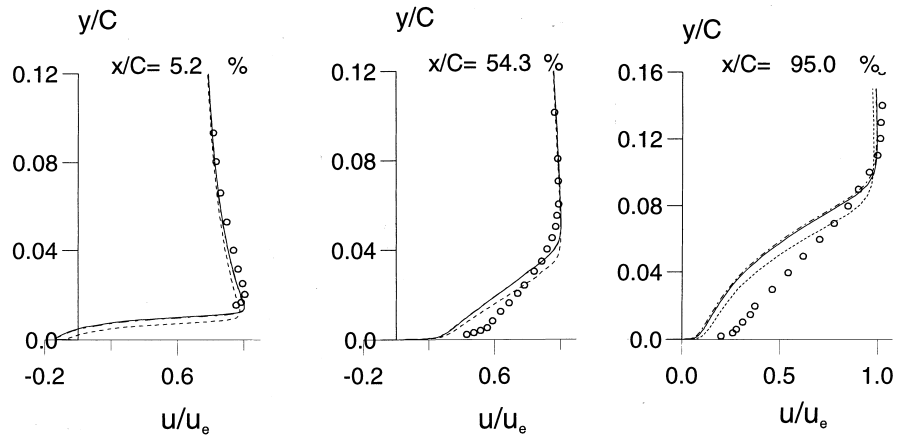

Fig. 2. Grid-independence test for the flow over the CD compressor blade with three different meshes. (——) 58 000 grid nodes; (- – -) 48 000 grid nodes; (- - -) 25 200 grid nodes.

mental data at all measured sections. The measurements suggest that the free-stream turbulence intensity at the leading-edge is 1.4 ± 0.2%. This guided the selection of Tu = 2% and $l_\varepsilon = 2.5$ mm at the inlet plane which is located at 0.5 of the chord upstream of the leading edge. With these values, the resulting decay of the free-stream turbulence intensity is in good agreement with the data. The same inlet conditions are also used for other inlet-flow angles.

4.3. Results for CD blade

Selected comparisons between predictions and experimental data are first given for the inlet angle $\beta = 40°$, and then for the maximum off-design value $\beta = 46°$. A comparison for the loss coefficient, given at the end of this section, encompasses the entire incidence-angle range listed in Table 2. A more extensive exposition is given in Chen (1996). Figs. 3–5 relate to $\beta = 40°$ and contain results for blade-surface pressure, streamwise velocity and turbulence intensity in the boundary layer along the suction side, integral boundary-layer quantities along both suction and pressure sides, and wake velocity. Fig. 3(c) shows that, while the suction-side boundary layer is subjected to deceleration by the action of the adverse pressure gradient, the flow remains attached (except for a small leading-edge separation bubble). All models return fairly close agreement with the experimental data for the surface-pressure distribution,

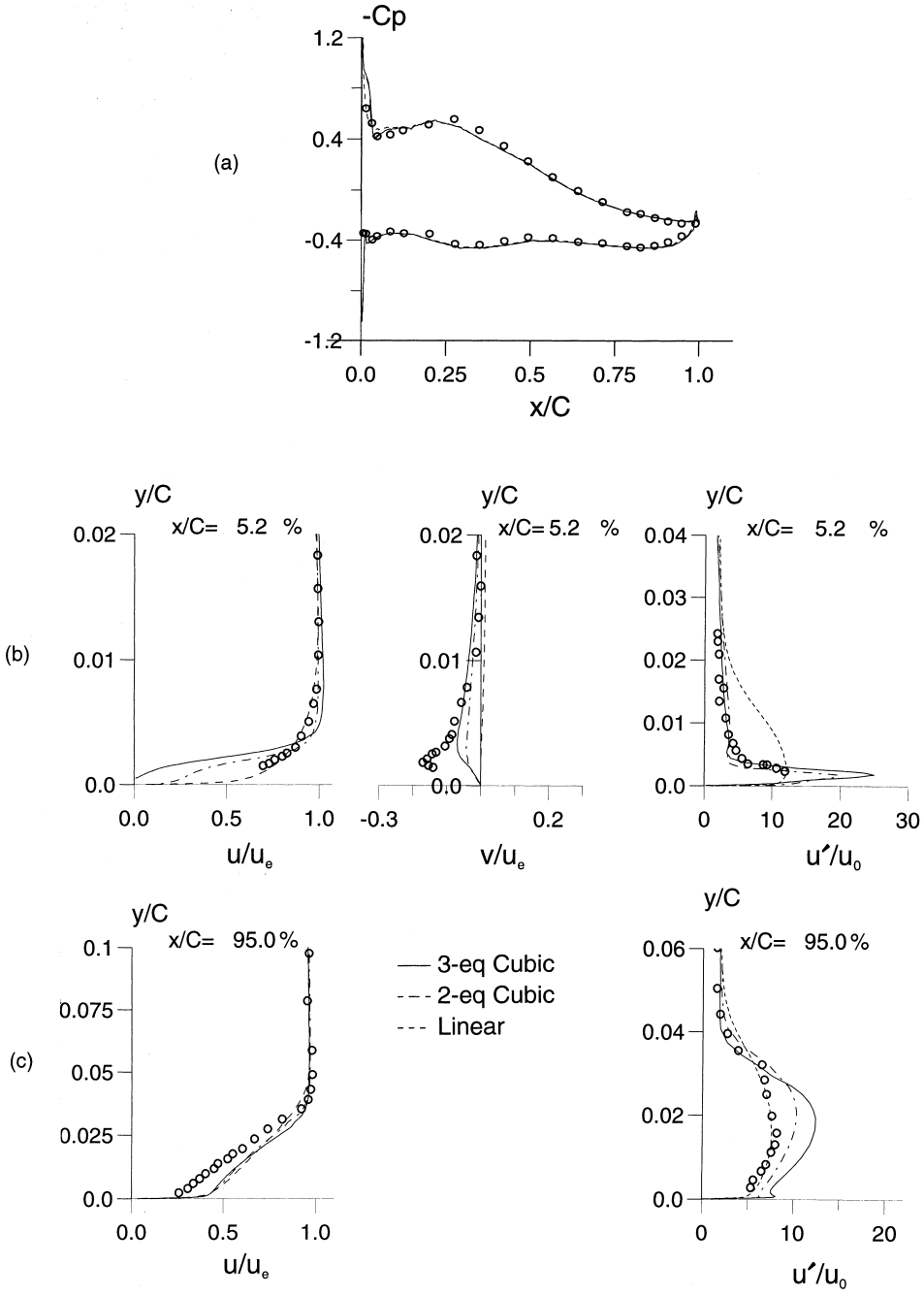

Fig. 3. CD compressor blade at $\beta = 40°$: (a) surface pressure distributions; (b) streamwise and transverse velocity profiles and streamwise turbulence-intensity profiles at $x/C = 5.2\%$ on the auction side; (c) streamwise velocity and turbulence-intensity profiles at $x/C = 95\%$ on suction side.

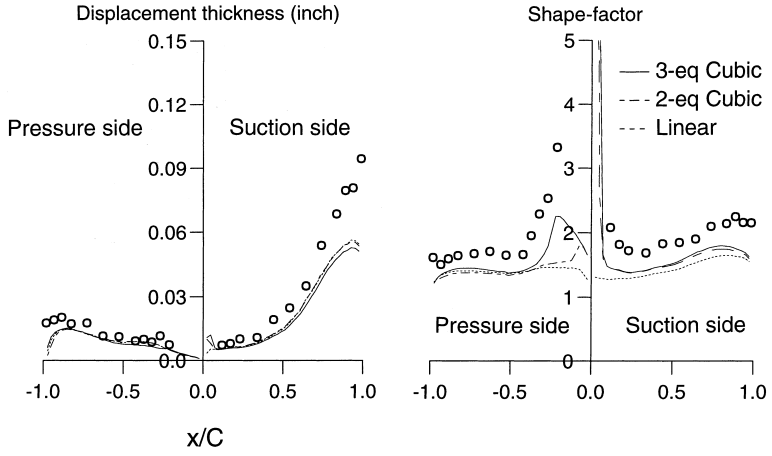

Fig. 4. CD compressor blade – boundary-layer displacement thickness and shape factor at $\beta = 40°$.

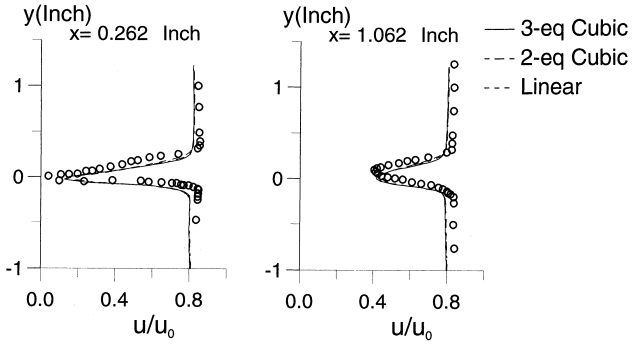

Fig. 5. CD compressor blade – wake mean-velocity profiles at $\beta = 40°$.

Fig. 3(a), except for the region around the leading-edge on the suction side. In this region, the large pressure peak signifies strong acceleration along the rounded leading edge following impingement. In reality, the leading-edge impingement is followed by a laminar separation which reduces the suction peak and provokes transition in the vicinity of the reattachment point at around 7% of chord. Elazar (1988) reported that it had been impossible to obtain measurements inside the laminar separation bubble as seeding particles, necessary for the LDA method, could not penetrate the separated region in sufficient numbers. However, an indication of the presence of the leading-edge separation is provided in Fig. 3(b) by the substantial, negative wall-normal velocity component at 5.2% of chord. The Launder–Sharma model is evidently unable to capture this leading-edge separation due to excessive turbulence-energy being generated by the impingement at the leading edge. The two non-linear models, on the other hand, predict this separation bubble, and this is reflected by the elevated negative near-wall normal velocity, shown in Fig. 3(b), as well as by the shape-factor distributions, Fig. 4, which will be discussed later. However, the predicted separation appears to be weak, especially that produced by the two-equation model, and its size is limited to a short region close to the leading edge. Thus, its effect is localised, and the C_p distribution further along the suction side is hardly affected by the separation. Since, for the design condition, the actual location of reattachment is quite close to the leading edge, transition occurs early and the boundary layer is fully turbulent over most of the suction surface. Hence, the Launder–Sharma model, although returning a fully turbulent unseparated flow, gives a reasonably good representation of the boundary layer downstream of the leading edge, as shown in Fig. 3(b). The two non-linear models capture the leading-edge separation, thereby predicting better results in the mid-chord portion of the boundary layer. Towards the trailing edge, however, all models return similar results which are all in good agreement with the measured data, Fig. 3(c), and which reflect the mildness of curvature and adverse pressure gradient, in addition to the insensitivity to leading-edge processes discussed above.

The profiles of turbulent intensity on the suction side, shown in Fig. 3(b), reveal that a seriously excessive level of turbulence is returned by the Launder–Sharma model near the leading edge due to the erroneously high generation of turbulence in the leading-edge impingement region. The non-linear models give, in contrast, similar levels of turbulence intensity, which are much closer to the data. Towards the trailing-edge, the non-linear models tend to predict excessive levels of near-wall turbulence. This is qualitatively consonant with the performance of the non-linear models in fully developed curved channel flow where a similar defect was observed (Suga, 1995). A contributory defect is the tendency of all models investigated herein to produce too high levels of turbulence intensity in adverse pressure gradient. While the Launder–Sharma model appears to give quite satisfactory accord with the experimental data for streamwise turbulence intensity at $x/C = 95\%$, it must be born in mind that this is partly due to the near-isotropy of the predicted intensity components and is also, fortuitously, linked to the wrong representation of the boundary-layer structure close to the leading edge.

The variations of the boundary-layer displacement thickness and its shape factor, shown in Fig. 4, imply marginal sensitivity to turbulence modelling, except for conditions at the leading edge. Before further comments are made on the computed integral boundary-layer parameters, it must be mentioned that the determination of these parameters is not straightforward and subject to some error. On the suction side, the edge velocity is normally identified by the maximum value which is readily determined. Hence, there is little ambiguity in identifying this quantity with reasonable accuracy. Particular difficulties arise, however, in evaluating the edge velocity next to the irrotational curved stream on the pressure side. Here, an approach recommended by Stock and Haase (1989) has been adopted, which entails the definition of the boundary-layer edge according to

$$\delta = 1.936 y|_{(y|\mathrm{d}u/\mathrm{d}y|)_{\max}}. \tag{8}$$

With the boundary-layer edge so determined, the distributions of displacement thickness and shape factor in Fig. 4 suggest that all models underestimate the tendency of the flow towards separation. On the pressure side, the results returned by the three-equation model are superior to those of the other two forms, partly because of the former model's reasonably adequate prediction of transition.

Since all models give very similar boundary-layer velocity distributions in the rear portion of the blade, there is no significant difference in the predicted wake-velocity profiles, as seen in Fig. 5. Compared with the experimental data, the free-stream velocity is slightly underestimated. This is because the models tend to under-estimate the suction-side boundary-layer and the displacement thickness near the trailing edge, leading to an insufficient lateral displacement of the wake. This defect may also be partly associated with the fact that the departure of the AVDR from unity reaches a maximum at this position. Thus, three-dimensional features, although still weak, are likely to be especially pronounced in the wake. Overall, however, the wake-velocity profiles returned by all models show good agreement with the experimental data, both in the near- and far-wake regions.

Comparisons for the flow angle $\beta = 46°$, the highest investigated by Elazar and Shreeve, are given in Figs. 6–8. Even at this extremely high incidence angle, the flow on the suction side does not separate at the trailing edge, signifying the favourable

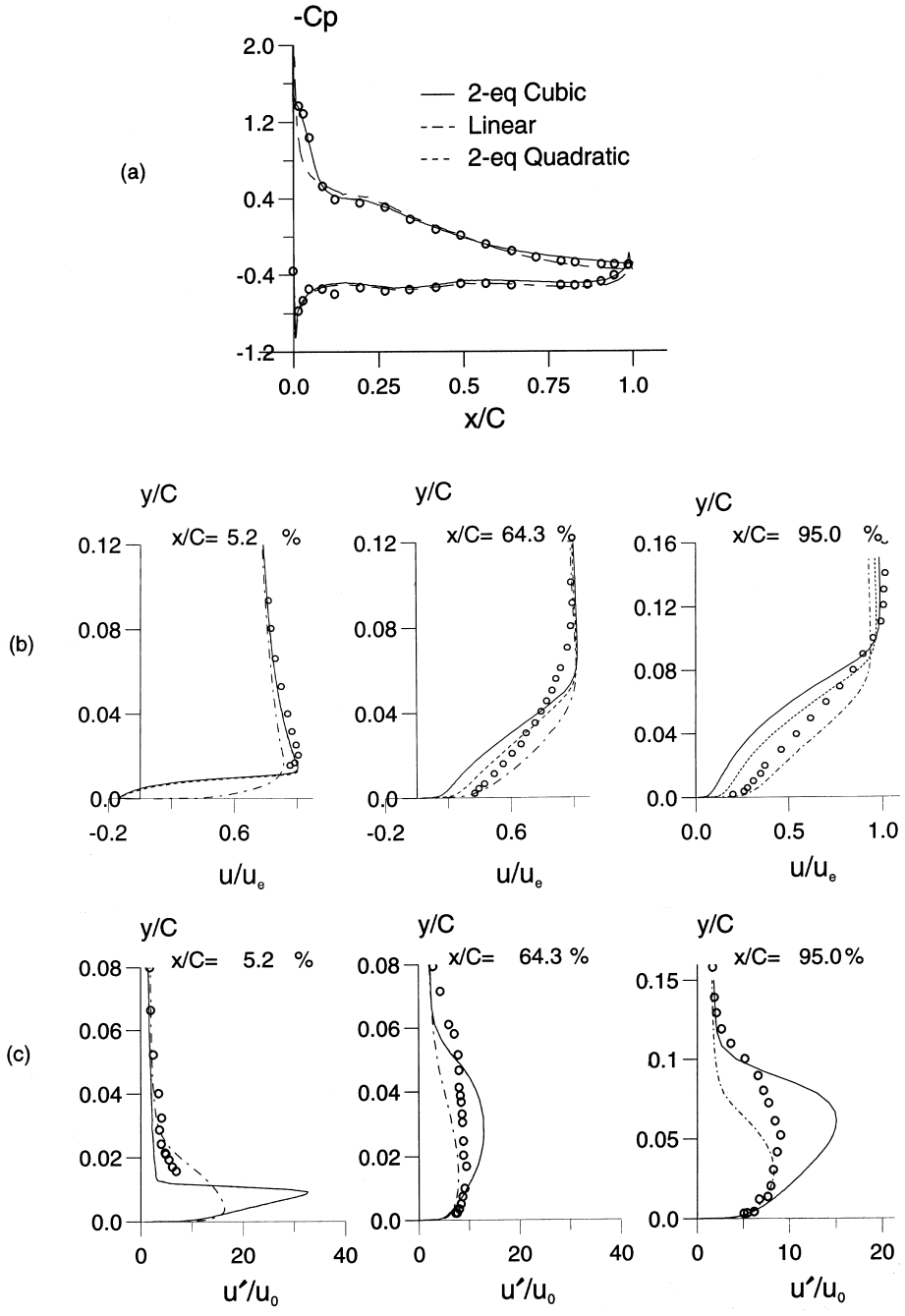

Fig. 6. CD compressor blade at $\beta = 46°$ – (a) surface-pressure distributions; (b) streamwise-velocity profiles on suction side; (c) streamwise turbulence intensity profiles on suction side.

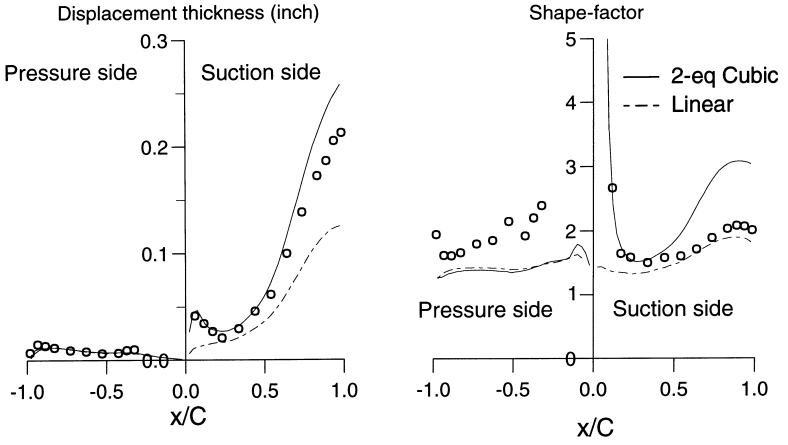

Fig. 7. CD compressor blade – boundary-layer displacement thickness and shape factor at $\beta = 46°$.

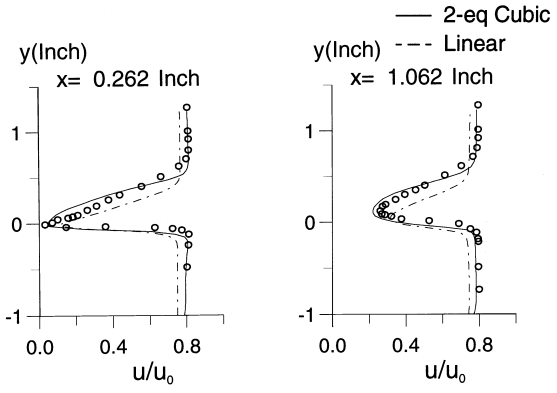

Fig. 8. CD compressor blade – wake mean-velocity profiles at $\beta = 46°$.

aerodynamic characteristics of the CD compressor blade. However, the leading-edge separation bubble on the suction side becomes extensive, stated by Elazar to occupy at least the first 20% of the chord, and this results in a steep increase in the loss. In addition, the flow is subjected to a strong adverse pressure gradient which would result, on its own, in a thick boundary layer towards the trailing edge. To compute this flow accurately, the leading-edge separation bubble must be resolved, and the correct response of the boundary layer to adverse pressure gradient and streamline curvature must be represented.

Unfortunately, at this largest incidence angle, the three-equation non-linear model could not be made to return a converged solution (although it does up to 43.4°). It appears that the main obstacle is the tendency of this model to predict a seriously excessive leading-edge separation bubble which occupies a substantial proportion of the suction side, thus provoking numerical instability which might be indicative of a tendency towards unsteadiness. Results arising only from the linear model and the two-equation non-linear form are thus presented below.

The measured pressure distribution, shown in Fig. 6(a), suggests the existence of a substantial leading-edge separation bubble covering about 15% of the suction side, which tends to diminish the steep adverse pressure gradient at that location. The two-equation non-linear model resolves this separation and thus returns a far better agreement with the experimental data at the leading edge. In contrast, the Launder–Sharma model fails, yet again, to predict separation, and hence returns a much too steep rise in pressure. Associated with the extensive differences in model performance at the leading-edge are the significant discrepancies observed in the trailing-edge region. Leading-edge separation results in a pronounced initial thickening of the boundary layer, and this has a marked influence on the boundary-layer structure further downstream, even if other response mechanisms in the attached flow portion are ignored. It is relevant to note here that computations on highly loaded, single-element aerofoils consistently show that a reduction in the suction-side pressure peak invariably leads to an elevation of the $-C_p$ tail at the trailing edge, as observed in Fig. 6(a). Thus, there appears to be, quite generally, a fairly sensitive coupling between the leading-edge and trailing-edge conditions, perhaps associated with the need to maintain constant circulation around the aerofoil or blade.

The superiority of the cubic model over the linear form, in terms of the prediction of the leading-edge separation, is evident from the streamwise-velocity distribution at $x/C = 5.2\%$, shown in Fig. 6(b). Further downstream, towards the trailing edge, the computed boundary layer is closer to separation than the measured one and has the wrong shape. The former reflects, at least in part, the elevated sensitivity to streamline curvature, which the non-linear model returns due to the inclusion of the cubic terms in the constitutive Eq. (2) (see also Eq. (3)). An indication of this sensitivity is provided in Fig. 6(b) by a comparison of the velocity profiles predicted with and without the cubic fragments (the latter identified in Fig. 6 by "2-eq Quadratic"). As expected, the exclusion of these fragments makes the flow less responsive to the adverse pressure gradient than that predicted by the full model. Although the Launder–Sharma model does not capture the leading-edge separation, it returns a very thick initial boundary layer, due to the excessive turbulence energy being generated during the impingement and deflection process, which then results in a rapid mixing and spreading in the outer part of the boundary layer. Towards the trailing edge, however, the model returns a thinner boundary layer than the experimental one, due to excessive mixing and hence insufficient sensitivity to and displacement by the adverse pressure gradient.

The variations of integral boundary-layer quantities, given in Fig. 7, demonstrate perhaps most strikingly the significant differences in the performance of the non-linear model relative to the linear form, and confirm previous conclusions that the former gives, overall, a superior representation of the flow, notwithstanding some disconcerting weaknesses. The most encouraging feature is the ability of the non-linear model to give a credible representation of the suction-side peak in the dis-

placement thickness that is associated with the leading-edge separation. Agreement is also good further downstream. However, as the trailing edge is approached, the displacement thickness grows too quickly. The shape factor computed by the non-linear model in the rear portion of the suction side is excessive, indicating that the boundary layer is too close to separation. Here again, this is entirely consistent with earlier observations made in relation to the velocity profiles in Fig. 6(b). The only major comment which can be made in relation to the pressure side is that the shape-factor variations imply that the non-linear model predicts transition to occur much too early. It must be recognised, however, that the experimental shape-factor data may be subject to significant error, especially in the vicinity of the leading edge, because these have been determined from very low values of displacement- and momentum-thickness data. As regards the performance of the linear model, it is clear that this model fails to give a credible description of the suction-side boundary layer: the leading-edge separation is not resolved, and the rate of increase in the displacement thickness is wrongly returned as a result of the insufficient sensitivity of the boundary layer to the adverse pressure gradient. The fact that the shape factor is correctly computed is fortuitous and reflects compensating errors in the displacement- and momentum-thickness solutions.

Results for the wake structure are given in Fig. 8. Here, the non-linear model gives much better accord with the experimental data for the velocity than the linear form, due principally to its ability to resolve the suction-side boundary layer more faithfully. In particular, the wake width and its lateral location are well represented by the non-linear model.

Of special interest to the designer is the variation of the total-pressure-loss coefficient

$$\omega = \frac{P_{T0} - P_{T2}}{P_{T0} - P_{D1}} \tag{9}$$

as a function of incidence, shown in Fig. 9. While the figure contains results arising from all three models examined in this study, the three-equation non-linear variant failed to return stable solutions at highly positive and negative incidence angles, i.e. $\beta = 24°$ and 46°. As seen, the different models give significantly different loss levels at off-design conditions. The linear model shows a far too low level of sensitivity of the loss to variations in the inlet angle, due to the fact that the boundary layer structure it predicts responds too weakly to the adverse pressure gradient acting on it. In contrast, the boundary layers computed by the non-linear models are thicker, are substantially affected by the leading-edge separation and respond considerably more sensitively to the adverse pressure gradient, thus giving rise to higher losses.

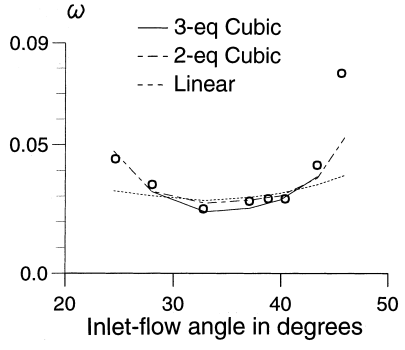

Fig. 9. CD compressor blade – distributions of total-pressure-loss coefficient.

4.4. DCA blade – geometry and computed flow conditions

The experimental data for the DCA blade used here have been obtained by Zierke and Deutsch (1989) who also give a detailed description of the geometry. In the experiment, three incidence angles were examined, namely 5.0°, −1.5° and −8.5°, thus covering a wide operational range and yielding boundary layers with a wide variety of characteristics. Sidewall suction was applied to keep the AVDR very close to unity, which ensured close adherence to two-dimensional conditions. The flow conditions at the three incidence angles are summarized in Table 3.

The blade's leading- and trailing-edge radii are both 0.914 mm (0.799% of chord length), giving an associated Reynolds number Re_d of about 4000. At such a low value, the non-linear models tend to predict extensive leading-edge separation and thus require a particularly fine grid to achieve a grid-independent solution. In addition, the experiment suggests that a massive trailing-edge separation exists even close to the design condition. To resolve this feature, it is thus also necessary to adopt a fine grid near the trailing edge. Fig. 10 shows the multi-block mesh surrounding the blade. The mesh size, in terms of the number but not distribution of grid nodes, and the block topology are essentially the same as those used for the CD-blade computations reported in the previous section. In the following, attention is focused on the incidence angle −1.5°. Results for other flow conditions may be found in Chen (1996).

4.5. Results for the DCA blade

Although the flow is at an inlet angle which departs by only −1.5° from the design condition, it is highly complex in comparison to the corresponding flow around the CD blade. On the suction side, there is a small leading-edge separation bubble, and this causes the flow to become turbulent close to the leading edge. Downstream, at about 80% of the chord, the turbulent boundary layer separates, forming a large recirculation zone which extends well beyond the trailing edge. On the pressure side, the boundary layer remains laminar up to a thin mid-chord separation region located at around 50% of the chord, which triggers transition around the reattachment point. To predict the flow accurately, all features associated with separation must be captured, since they either provoke transition or produce a large boundary-layer displacement. In addition, the significant streamline curvature induced by the highly curved blade surface and the strong adverse pressure gradient acting on the suction-side boundary layer introduces further complexities to the flow field. The present flow is, therefore, highly challenging.

On the basis of test calculations, the turbulence intensity and length scale have been chosen as $Tu = 2\%$ and $l_\varepsilon = 4.5$ mm, respectively, and these give the correct turbulence levels at the edges of the boundary layers at locations for which measurements are available.

Comparisons between the numerical solution and experimental data are shown in Figs. 11 and 12. The C_p variation given in Fig. 11(a) already implies that the suction-side boun-

Table 3
DCA blade – flow conditions investigated

Case	Incidence angle (degree)	Re_c	Re_d
1	5.0	505 000	4040
2	−1.5	501 000	4008
3	−8.5	507 000	4056

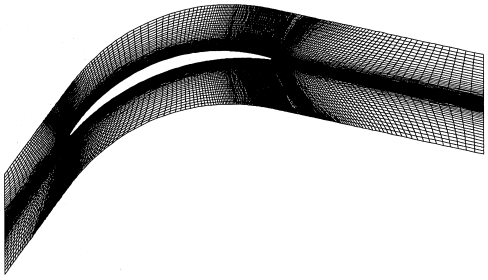

Fig. 10. Computational grid for DCA compressor blade.

dary layer has not been well represented, especially that towards the trailing edge. The leading-edge separation for this case is small, and the flow reattaches within a distance of 3–4% of chord, as is signified by the spike on the lower curve in Fig. 11(a). This spike, albeit weaker, is also observed experimentally, and it is only the non-linear models which resolve it. The experimental C_p distribution on the suction side features a distinct plateau beyond 80% of chord, indicating the presence of a massive trailing-edge separation. However, this plateau is not returned by any of the models, as none is able to capture the separation of the boundary layer.

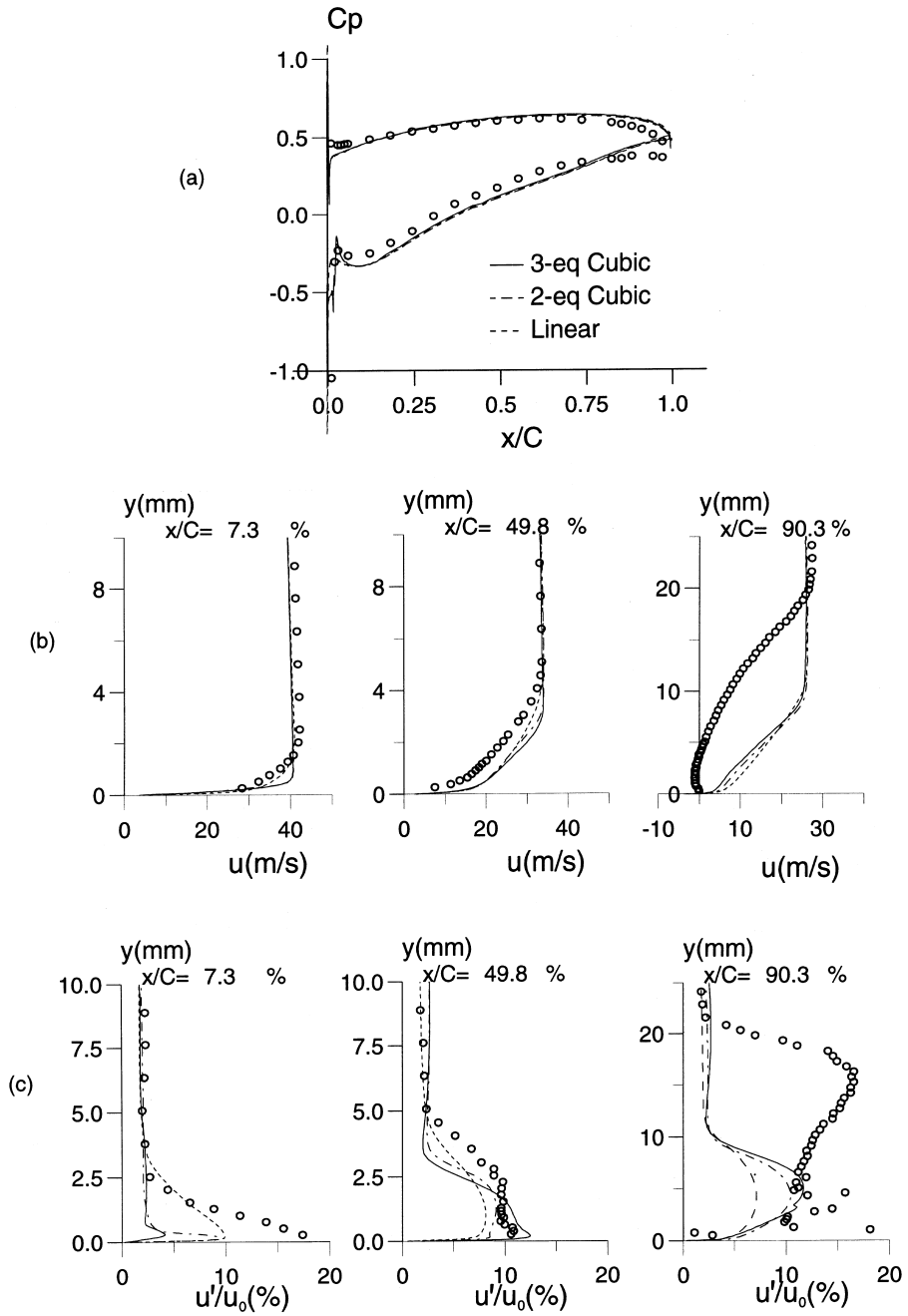

Fig. 11. DCA compressor blade at $i=-1.5°$ – (a) surface-pressure distributions; (b) streamwise-velocity profiles on suction side; (c) streamwise turbulence-intensity profiles on suction side.

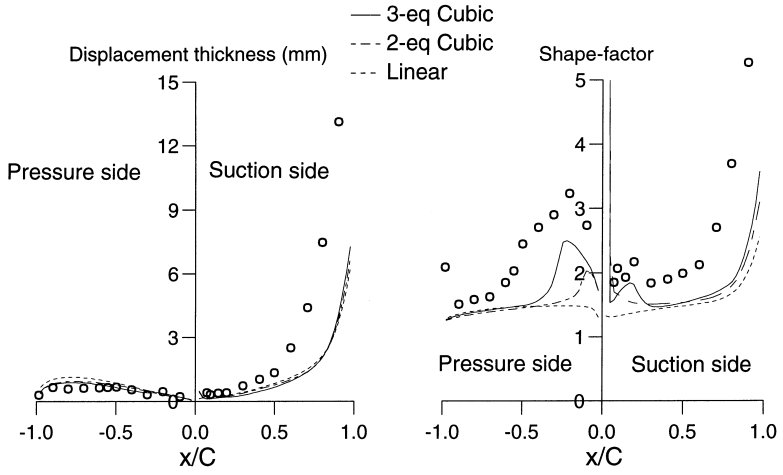

Fig. 12. DCA compressor blade – boundary-layer displacement thickness and shape factor at $i=-1.5°$.

The experimental velocity and turbulence-intensity profiles at $x/C=7.3\%$, shown in Fig. 11(b) and (c), respectively, suggest that the boundary layer is already fully turbulent at this location. The linear model, although failing to predict the leading-edge separation, returns better agreement with the data than the other two non-linear variants, but this is fortuitous. Moreover, this model does not respond adequately to curvature and adverse pressure gradient, and hence underestimates the boundary-layer thickness as the flow progresses downstream. Thus, in common with earlier experience, the linear model predicts a boundary layer which is too turbulent and which resists separation. The performance of the non-linear models is, unfortunately, equally disappointing, although it seems due to different defects. As already noted, these models capture the leading-edge separation, but the velocity and turbulence-intensity profiles at $x/C=7.3\%$, and others not included here, suggest that the predicted boundary layer does not become fully turbulent up to $x/C=20\%$, well beyond the experimental reattachment. As the pressure gradient acting over this portion of the suction side is weak, an unrealistically thin boundary layer with a low level of turbulence is predicted in the early stages of the flow development. The misrepresentation of the boundary layer further downstream is aggravated by what appears to be insufficient mixing in its outer part. This defect inhibits displacement and results in the boundary layer remaining thin and highly turbulent close to the wall, thus preventing suction-side separation despite the turbulence-attenuating effect of streamline curvature (see Fig. 6(b)).

The complexity of the flow on both the suction and pressure sides is also conveyed by the variations of boundary-layer quantities, especially the shape-factor distributions given in Fig. 12. On the suction side, the small leading-edge separation bubble is barely resolved by the measurement, its existence being reflected by the slightly elevated shape factor. The rather low level of shape factor near the leading edge suggests a rapid recovery from the separation, while the steep rise from $x/C=0.75$–0.8 to the trailing edge indicates the presence of trailing-edge separation. On the pressure side, the magnitude of the measured shape factor is well above the value expected for turbulent boundary layers up to $x/C=0.75$, at which location the rapid decline implies the onset of transition. Since the mid-chord separation is short and very thin, it does not manifest itself by more than a hint in the shape-factor distribution. Clearly, the most serious predictive defect in this case is the failure of all models to capture the suction-side separation, and this is reflected by substantial discrepancies between the predicted and measured displacement thickness and shape factors. [1] Only the three-equation model provides a credible representation of the transition in the pressure-side boundary layer. The observation that the linear model returns a broadly correct boundary-layer thickness (not shown) in the initial 50% of the suction side, coupled with an insufficient increase in the displacement thickness (see Fig. 12), suggests that the failure of this model to resolve the suction-side separation is rooted in an excessive level of turbulent mixing in the boundary layer, aggravated by premature transition. The process responsible for the failure of the non-linear variants is not clarified by the integral parameters included in Fig. 12. Previous arguments, based on profiles of turbulence intensity, led to the conclusion that the non-linear models predicted a substantial delay in the onset of transition, hence returning an unrealistically thin boundary layer which, once turbulent, resisted separation. The integral quantities given in Fig. l2 do not offer obvious support for this argument. However, it has been observed that the non-linear models, especially the three-equation variant, gives a broadly correct *rate* of increase in boundary-layer thickness, following transition, but a far too low rate of increase over the first 20–30% of the chord. Yet, the increase in the displacement thickness is clearly under-estimated, reflecting an insufficient response of the inner boundary layer to the adverse pressure gradient. This behaviour thus lends some support to earlier arguments, based on velocity and turbulence profiles, on the origins of the failure of the non-linear models to predict the rear suction-side separation.

5. Conclusions

The paper investigated the performance of three low-Re turbulence models, one linear and two non-linear, when applied to the flow over two compressor cascades, a CD and a DCA configuration. The multi-block method reported in Lien et al. (1996) has been exploited to facilitate accuracy through the use of a nearly orthogonal, O-type grid surrounding the blade surfaces, thus avoiding distorted grids in the near-wall region. In addition, very fine meshes were used to maximise

[1] Recent second-moment computations presented by Chen et al. (1997b) have been found to capture this separation well.

the numerical resolution in some highly influential separated-flow areas.

In the case of the CD compressor blade operating close to the design condition, all models perform similarly well, and the results are in good agreement with the measured data. This is due to the absence of separation and to the relative simplicity of the strain field within the fairly thin boundary layers. In off-design conditions, the non-linear models generally yield superior results to those returned by the linear model, as the former group capture the leading-edge separation and are able to represent more realistically the growth of the boundary layer under the action of adverse pressure gradient and streamline curvature. The non-linear models also give a better representation of the wake structure, as they predict more realistically the boundary layers towards the trailing edge, especially the one which is preceded by a substantial leading-edge separation.

An adverse characteristic of the particular non-linear forms examined here is their inferior numerical stability relative to the linear form. In fact, the three-equation form failed to converge at large off-design inlet incidence. This does not, however, appear to be a consequence of inherent, numerically disadvantageous properties of the models, but may rather be rooted in the models' tendency to seriously overestimate the size of the leading-edge separation. This reflects a trend towards predicting low levels of turbulent viscosity in the separated shear layer, which promotes unsteadiness in the computation and thus prevents convergence of the steady-state computational scheme.

In terms of loss predictions, the non-linear models give more realistic levels than the linear form, especially at off-design conditions, although the computed loss levels are not satisfactory. The failure of the linear formulation is due to its inability to capture leading-edge separation and thus the structure of the downstream boundary layer.

The flow over the DCA compressor blade is highly complex, even close to the design condition. It features several separation and transition events which are all influential. None of the models investigated here is able to capture these important flow phenomena with a sufficiently level of realism. Hence, the results are generally not in good agreement with the data.

Since Re_d, the Reynolds number based on the leading-edge radius, is especially low in the DCA geometry, the non-linear models tend to give an excessive leading-edge separation bubble, and this is consistent with observations made in relation to transitional flow over a flat plate with rounded leading edge (see Chen, 1996). The misrepresentation of the leading-edge separation results in large discrepancies between the predictions and the data after reattachment. Hence, the downstream flow region is badly resolved, regardless of the models' intrinsic ability to represent more realistically than the linear forms the sensitivity of the fully turbulent boundary layer to streamline curvature.

References

Apsley, D.D., Leschziner, M.A., 1997. A new low-Re non-linear two-equation turbulence model for complex flows, Proceedings of the 11th Symposium on Turbulent Shear Flows. Grenoble, France, pp. 6–25.

Chen, W.L., 1996. Turbulence modelling for highly-loaded cascade blades. Ph.D. Thesis, UMIST, Manchester, UK.

Chen, W.L., Lien, F.S., Leschziner, M.A., 1997a. Local mesh refinement within a multi-block structured-grid scheme for general flows. Comp. Meth. Appl. Mech. Eng. 144, 327.

Chen, W.L., Lien F.S., Leschziner, M.A., 1997b. Computational modelling of highly-loaded compressor cascade flows. Proceedings of the 11th Symposium on Turbulent Shear Flows. Grenoble, France, pp. 1–13.

Craft, T.J., Launder, B.E., Suga, K., 1993. Extending the applicability of eddy-viscosity model through the use of deformation invariant and non-linear elements. Proceedings of the Fifth International Symposium on Refined Flow Modelling and Turbulence Measurements. Paris, p. 125.

Craft, T.J., Launder, B.E., Suga, K., 1997. Prediction of turbulent transitional phenomena with a nonlinear eddy-viscosity model. Int. J. Heat Fluid Flow 18, 15.

Elazar, Y., 1988. A mapping of the viscous flow behaviour in a controlled diffusion compressor cascade using laser Doppler velocimetry and preliminary evaluation of codes for the prediction of stall. Ph.D. Dissertation, Naval Postgraduate School, Monterey, California.

Elazar, Y., Shreeve, R.P., 1990. Viscous flow in a controlled diffusion compressor cascade with increasing incidence. ASME, J. Turbomachinery 112, 256.

Kim, J., Moin, P., Moser, R., 1987. Turbulence statistics in fully developed channel flow at low Reynolds number. J. Fluid Mech. 117, 113.

Launder, B.E., 1989. Second-moment closure: present... and future? Int. J. Heat Fluid Flow 10, 282.

Launder, B.E., Sharma, B.I., 1974. Application of the energy-dissipation model of turbulence to the calculation of flow near a spinning disc. Int. J. Heat Mass Transfer 1, 131.

Leonard, B.P., 1979. A stable and accurate convective modelling procedure based on quadratic upstream interpolation. Comput. Meth. Appl. Mech. Eng. 19, 59.

Leschziner, M.A., 1994. Refined turbulence modelling for engineering flow. Computational Fluid Dynamics'94, Wiley, New York, p. 33.

Lien, F.S., Chen, W.L., Leschziner, M.A., 1995. Low-Reynolds-number eddy-viscosity modelling based in non-linear stress–strain/vorticity relations. Proceedings of the Third Symposium on Engineering Turbulence Modelling and Measurements. Crete, Creece, p. 91.

Lien, F.S., Chen, W.L., Leschziner, M.A., 1996. A multi-block implementation of a non-orthogonal, collocated finite volume algorithm for complex turbulent flows. Int. J. Numer. Methods Fluids 23, 567.

Lien, F.S., Durbin, P.A., 1996. Non-linear k-ε-v^2 modelling with application to high-lift. Proceedings of the Summer Programme. Centre for Turbulence Research, Stanford University, USA.

Lien, F.S., Leschziner, M.A., 1994a. A general non-orthogonal collocated FV algorithm for turbulent flow at all speed incorporating second-moment closure, Part 1: computational implementation. Comp. Meth. Appl. Mech. Eng. 114, 123.

Lien, F.S., Leschziner, M.A., 1994b. A general non-orthogonal collocated FV algorithm for turbulent flow at all speed incorporating second-moment closure, Part 2: application. Comp. Meth. Appl. Mech. Eng. 114, 149.

Lien, F.S., Leschziner, M.A., 1994c. Upstream monotonic interpolation for scalar transport with application to complex turbulent flows. Int. J. Numer. Methods Fluids 19, 527.

Lien, F.S., Leschziner, M.A., 1996. Second-moment closure for three-dimensional turbulent flow around and within complex geometries. Computers and Fluids 25, 237.

Nisizima, S., Yoshizawa, A., 1987. Turbulent channel and Couette flows using an anisotropic k-model. AIAA J. 25 (3), 414.

Pope, S.B., 1975. A more general effective-viscosity hypothesis. J. Fluid Mech. 72, 331.

Rubinstein, R., Barton, J.M., 1990. Non-linear Reynolds stress models and the renormalisation group. Phys. Fluids A 2, 1472.

Sanger, N.L., 1983. The use of optimization techniques to design controlled-diffusion compressor blading. ASME, J. Eng. for Power 105, 256.

Savill, A.M., 1991. Turbulence model predictions for transition under free-stream turbulence. Progress Report Poster Paper at RAeS Transition and Boundary Layer Control Conference. Cambridge.

Shih, T.H., Zhu, J., Lumley, J.L., 1993. A realizable Reynolds stress algebraic equation model. NASA TM-105993.

Speziale, C.G., 1987. On nonlinear k-l and k-ε models of turbulence. J. Fluid Mech. 178, 459.

Stock, H.W., Haase, W., 1989. Determination of length scales in algebraic turbulence models for Navier–Stocks methods. AIAA J. 27, 5.

Suga, K., 1995. Development and application of a non-linear eddy-viscosity model sensitized to stress and strain invariant. Ph.D. Thesis, UMIST, Manchester, UK.

Zierke, W.C., Deutsch, S., 1989. The measurement of boundary layers on a compressor blade in cascade. NASA C.R.-185118.